15.7 AN ANALYSIS OF TROPICAL CYCLONE FORMATIONS IN THE SOUTH CHINA SEA DURING THE LATE SEASON

YUNG-LAN LIN*[1, 2] AND CHENG-SHANG LEE[1]
[1]Taipei Aeronautic Meteorological Center, Civil Aeronautics Administrator, Taipei, Taiwan
[2]Department of Atmospheric Sciences, National Taiwan University, Taipei, Taiwan

1. INTRODUCTION

During the boreal winter, eastern Asia is dominated by a strong and steady monsoon, which develops as the continent cools and the Siberian anticyclone strengthens. Previous studies have shown that the northeasterly cold surge that comes off of Asia leads to an intensification of convective disturbances in the near-equatorial region. These disturbances, which may have originated from the semi-stationary near-equatorial trough over the coast of north Borneo or from a westward propagating wave in the western North Pacific (WNP) can intensify and become a tropical cyclone (TC) (Chang et al 1979). For example, tropical storm (TS) 29w and one of the most near-equatorial Typhoon Vamei which formed in the southern SCS during the boreal winter of 2001 were associated with the northeasterly cold surges are from the semi-stationary near-equatorial trough. Chang et al. (2003) noted that the formation of Vamei was associated with an interaction of an exceptionally strong and persistent northwesterly cold surge that created the large background cyclonic vorticity at the equator, and a weak Borneo vortex that drifted into the southern tip of the South China Sea. They reasoned that while the cold-surge and Borneo vortex events are both common during the boreal winter, the shift of the vortex center such that much of the cyclonic circulation lies over land contributes to the fact that it is extremely rare for the vortex to intensify and organize as a TC.

From 1972 to 2005, about one thousand TCs formed in the WNP. During the same period, 131 TCs formed in the SCS, with an annual average of 3.9. Almost no TC formation occurs in the SCS from January to March, but the number of TC formations increases significantly in May and June (mei-yu season) and accounts for 18.3% of the total number of TCs in the SCS. This number is significantly higher than that (9.7%) in the WNP. Similar situation occurs in December during which the percentage of storm formations is 8.4% for the SCS but is only 4.6% for the WNP. Also the monthly formation rates in the WNP decrease gradually from August to February while in the SCS a second maximum occurs in December. Lee et al. (2008) examined the mesoscale features of 124 TC formations in the WNP during 1999–2004. Based on low-level wind flow and surge direction, the formation cases are classified into six synoptic patterns. The monthly distribution of the six flow patterns suggests that the northeasterly cases, 15 % of total, may be related to the cold surges in the SCS during Asian winter monsoon.

The unique topography of the southern SCS, which includes the Malay Peninsula and Borneo, acts to channel the flows toward the equator. Cold surge winds are dry, but are moistened significantly at the southern SCS due to the long overwater trajectory. The gradient of planetary vorticity together with blocking and deflection due to topography may contribute to TC formations such as the equatorial typhoon Vamei in 2001 (Chang et al., 2003). Additionally, the interactions among the synoptic-scale Borneo vortex, northeasterly cold surge, and the intraseasonal Madden-Julian oscillation (MJO) during the boreal winter contribute to the variability of deep convections in the region (Chang et al. 2005).

Corresponding author address: Yung-Lan Lin, Department of Atmospheric Sciences, National Taiwan University, 1, Section 4, Roosevelt Rd., 106 Taipei, Taiwan.
E-mail: ryanlin@nat.as.ntu.edu.tw

2. DATA

Data from various sources are used in this study. First, the climatology of TC formations in the SCS during 1972–2005 is based on the best-track data from the JTWC. The daily weather charts of JMA are used to address the surface features. Additionally, the infrared and visible satellite imageries from the Geostationary Meteorological Satellites (GMS), Geostationary Operational Environmental Satellite-9 (GOES-9) and Multi-functional Transport Satellite (MTSAT-1R) in the same 34-yr period are examined as a comparison with the surface features. The daily mean interpolated outgoing longwave radiation (OLR) with a 2.5° latitude/longitude resolution is taken from the National Oceanic and Atmospheric Administration (NOAA). The six-hourly National Centers for Environmental Prediction (NCEP) reanalyses with the same resolution are used to analyze the upper-level features. To monitor the MJO activity, Wheeler and Hendon (2004) developed a seasonally independent index which is based on a pair of empirical orthogonal functions (EOFs) of the combined fields of near-equatorially averaged 850-hPa zonal wind, 200-hPa zonal wind, and satellite-observed outgoing longwave radiation (OLR) data.

3. CHARACTERISTICS OF SCS TC FORMATION DURING THE LATE SEASON

During the period of 1972-2005, twenty two TCs formed in the SCS during the late season (only one case in January). Eleven of these storms originated from the

disturbances located in the southern SCS and are classified as semi-stationary cases. The others were associated with westward-propagating disturbances which originated in the WNP and passed the Philippines. These systems are classified as westward-moving cases. The best tracks of these two types of cases reveal that the moving directions of semi-stationary cases are more diversified when compared to those of the westward-moving cases. The westward-moving cases generally are located to the south of the subtropical high where stable easterly prevail. Many semi-stationary cases, however, are located at the western edge of the subtropical high where the steering flow is less well-defined. Therefore, the systems might move toward different directions, westward, northward or even eastward.

The average maximum intensities are 44 kt and 46 kt for semi-stationary and westward-moving TCs, respectively. These numbers are about the same as that (43 kt) of the typical frontal-type formation case (Lee et al., 2006). However, they are significantly smaller to those of TCs in the WNP due to the smaller water mass in the SCS. For those cases which develop to TS intensity, the time periods from the first 25 kt to 35 kt are 28 h and 21 h for the semi-stationary and westward-moving cases. These numbers are much smaller than that (47 h) for the typical frontal-type formations. They are also smaller than those of TCs in the WNP during the mei-yu (35.7 h) and late (36.4 h) seasons. In other words, the initial development of a TC in the SCS is relatively faster especially for the westward-moving cases.

4. COMPOSITES OF FORMATION AND NONFORMATION CASES

To help understand the formation process of a TC in the SCS during the late season, it is important to also examine those disturbances which developed to a well-recognized stage but do not develop to TCs (hereafter termed the nonformation cases). Therefore composite of the nonformation cases are studied and compared against that of the semi-stationary cases (hereafter termed the formation cases).

To examine the general environments of the formation and nonformation cases, composites are done for the 11 formation cases and 33 nonformation cases using the NCEP reanalysis. Composite analyses show that eleven of formations originated from the southern SCS and the 33 nonformation cases have a closed surface isobar that lasts for at least 48 h but does not develop into a TD. For the nonformation cases, the time when the closed surface isobar first formed is referred as the zero-time reference (Lee et al. 2006). This applies to the composites of the formation cases as well so that they do not have a higher intensity when compared with the nonformation composites. The low level disturbance near the coast of North Borneo and one-third of the low level circulations located at the Borneo landmass did not develop further after 36 h of the zero-time reference once they reached the maximum relative vorticity (Fig. 1b). During the boreal winter at low level troposphere in the SCS, there is cyclonic shear at the left side of the northeasterly. But the northeasterly are accompanied by a cold surge north of the nonformation cases, which are weaker in magnitude and the environmental cyclonic vorticity in the southern SCS is weaker than that of formation cases.

The midlevel (500 hPa) circulation shows that 48 h after the zero reference time, it is clear that the subtropical high ridge extends just over the SCS for nonformation (Fig. 2b), which is similar to the westward-moving case (Fig. 7b). The displayment of positive vorticity is contracted closer the Borneo landmass. For the formation group, however, the subtropical high only dominates east of 120° E, not the SCS so that deep convection is not suppressed (Fig. 2a). Upper level (200-hPa) divergent flow demonstrates that although a similar diffluent structure exists at upper levels as in the formation and nonformation cases, the divergent flow over the southern SCS that is associated with the anticyclone provides an upper-level environment that is conducive to formation (Fig. 2c).

To compare the convection distribution during the formation process, the OLR comparison between formation (Fig. 3a) and nonformation (Fig. 3b) cases is presented. Two days before to three days after the zero-reference time, in the formation cases, the lower area of OLR located in the southern SCS and extending to the entire maritime continent. In contrast, the convection in the nonformation cases is always weaker and less widespread in the southern SCS (Fig 3b).

The scatter plot for 925-hPa relative vorticity and 200-hPa divergence reveals that the distribution between formation and nonformation cases is separable at early formation process (Fig. 4a). At the latter formation process, it is more significant (Fig. 4b). Due to the decreasing of vertical wind shear and increasing of 700-hPa relative humidity, the distribution at early formation process (Fig. 4c) is broad than these at latter formation process. Meanwhile the 700-hPa relative humidity in formation cases is always higher than that in nonformation cases (Fig. 4d). The statistics also shows that 83.2 % of formation, the 925-hPa relative vorticity is above 2.49×10^{-5} s^{-1} (average vorticity minus one standard deviation), only 44.8 % of nonformation is above the value. For 700-hPa relative humidity, the formation is greatly larger than nonformation (83.9 % v.s. 8.6 %). For general the vertical wind shear of nonformation is stronger than that of formation, but the difference of percentage (the value is above average vertical wind shear plus one standard deviation, 14.7 m s^{-1}) is smaller. Also the difference of 200-hPa divergence is not significant.

Aerial averages of several quantities can also distinguish the environmental conditions in which formation and nonformation are embedded. The average 925-hPa relative vorticity within a 500-km radius that is centered on the surface pressure minimum for the formation cases maintains a magnitude between $2.7 \times$

10^{-5} s^{-1} to 3.5×10^{-5} s^{-1} after the reference time (Fig. 5a). It is larger than that of a typical frontal-type formation (2×10^{-5} s^{-1} to 3×10^{-5} s^{-1}). However the nonformation cases have a smaller magnitude of 925-hPa vorticity (2×10^{-5} s^{-1} to 2.5×10^{-5} s^{-1}) for the duration of time. Both of magnitude changes for formation and nonformation cases is small during the entire duration. The result of genesis potential (850-hPa minus 200-hPa relative vorticity; McBride and Zehr 1981) change is similar to the 925-hPa relative vorticity. The 200-hPa divergence associated with the formation case continues to be high 36 h after (about the time of reaching 25kt) the reference time, which is favorable for further intensification of the TD (Fig. 5b). In contrast, the divergence associated with the non-formation case is smaller throughout the period. The low level relative humidity is also different between the formation and nonformation, especially the 700-hPa relative humidity reveals that formation is increasing above 85 % at latter formation process and it is always 15 % higher than nonformation (Fig. 5c). The average 200–850-hPa deep environmental-vertical wind shear (within a radius from 500 to 900-km) for the nonformation cases (Fig. 5d) is 2–3 m s^{-1} smaller than it is for the formation cases at the zero-reference time. The formation case also has a similar decrease in the magnitude of vertical wind shear throughout the period. Although the climatological flow of winter monsoon is that the strong 200-hPa southwesterly over low level northeasterly create larger vertical wind shear in the region, where the values of vertical wind shear for the formation cases during the late season is 2-4 m s^{-1} larger than it is for the typical frontal-type formation cases associated with the mei-yu front, the tendency of decreasing vertical wind shear is more favorable for development.

Whatever the 925-hPa composite of nonformation and formation cases, the background northeasterly are pretty strong with a value of 13-15 m s^{-1} is over the western SCS. Aerial averages of 925-hPa total wind of northeasterly are about 11 m s^{-1} for formation at the zero-reference time (Fig. 6c). At about 36 h, which is around the time that formation cases reach 25kt, it is decreasing. At 60 h, when it is a developing tropical storm, it intensified again. However, the nonformation case has no significant change in magnitude during the duration. In the 925-hPa composite, the center of the vortex is oriented along the western Borneo coastline. Chang et al. (2005) explained that although the presence of the surge acts to increase the strength of the vortex, the surge results in a shift of the vortex center from being located over the southern SCS to being near the Borneo landmass. Therefore, the decreasing northeasterly at 30 h after the zero-reference time prevents the shift of the low-level circulation center of the formation cases from the southern SCS to a location near the Borneo landmass.

The difference between northeasterly in the formation and nonformation cases shows (Fig. 6a) that there has a one-time significant intensification before 30 h and a one-time significant weakening within approximately 30h to 60h. As for the space distribution, the maximum occurs at about 30 h in the eastern SCS and then a significant weakening follows until that at 60 h. There is a minimum area at 120°E. The sequence is similar to the results for aerial averages of 925-hPa northeasterly (Fig. 6c). However the difference between formation and non-formation is minor (about 1-2 m s^{-1}). In order to realize the differences whether is significant or not, the T-test statics and trend is presented. In Fig 6b, the 925-hPa wind vector is mean flow of formation minus nonformation during the weakening of northeasterly (30 to 60 h), the cyclonic circulation is still located at north of Borneo, but the negative tendency of northeasterly in the northern SCS is significant. Also near the equatorial SCS is negative with 2 m s^{-1}.

The distribution of positions is also consistent with the change of northeasterly. The position at 30 h of formations (Fig. 7a) gradually moves northward away from the Borneo coastline when the northeasterly are significantly decreasing at 60 h (Fig. 7b). However, the change of the northeasterly for nonformation is too minor to affect its low level circulation shift, it is no obvious southwestwardly or northwardly motion. (Fig. 7c-d).The tendency difference of 925-hPa relative humidity shows that it is positive during the early formation process at the eastern SCS and there are two maximum in the west of Borneo and Luzon (Fig. 8a). Because cold and dry northeasterly flow experience a warm water in the eastern SCS that results in moistening the low level troposphere. Moreover there is a negative minimum over the Vietnam landmass. While the weakening of northeasterly after 30 h in the northern SCS, it is negative in the northwestern SCS during the latter formation process (Fig. 8b). Meanwhile the strong northeasterly axis is also in the western SCS (Fig. 1). This allows formation cases not be weakened by the cold and dry air incursion along the Vietnam coast. The result is similar to Chang et al. (1979).

5. DISCUSSION AND CONCLUSIONS

Among the 131 TC formations in the SCS during 1972–2005, 22 occurred from November to January. In addition, 11 of these were from the Pacific and steered by the easterly of subtropical high, moving to the SCS, while the remaining 11 were semi-stationary and developed originally in the southern SCS. In contrast, 33 nonformation cases in the SCS during the period of 1972-2005 were identified in order to distinguish them from the 11 semi-stationary formation cases. These are cases with a similar low-level circulation origin, namely, from the southern SCS near the coast of north Borneo. In these, the vorticity in the southern SCS is smaller. Because of the influence of a strong subtropical high, deep convection is suppressed in the SCS. Although a similar, diffluent structure exists in upper levels as in the semi-stationary formation, it appears that the development and divergence over the low-level disturbance is weaker. At the early state of formation process, the stronger northeasterly is favorable for

formation cases to induce larger cyclonic vorticity environment in the southern SCS. However the strong northeasterly at the latter formation process may also result in the system becoming too close to the Borneo landmass. Also it may lead the cold and dry air incursion along the Vietnam coast to suppress convection due to stabilizing effect. The early formation period shows the larger westerly vertical wind shear (Fig. 9a) and low-level north wind located at the northern SCS with strong cold advection (Fig. 9b). The latter formation period shows that the largest humid difference near 700 hPa reaches 15 % and there is a warm core anomaly near 500 hPa accompanying the stronger updraft. Moreover the low-level cold advection at the northern SCS and the vertical wind shear also weaken (Fig. 9c and d). Whereas the nonformations experience smaller vertical wind shear (about 7 m s^{-1}) than the formations during the early period, later they continually increase and become larger than the formations. Moreover, the climatological flow of the winter monsoon is that the strong 200-hPa southwesterly over low level northeasterly cause larger vertical wind shear in the region, where the values of vertical wind shear for the nonformation cases during the late season is 2-4 m s^{-1} larger than for the typical frontal-type formation cases.

Comparing the probability of TC formation between the mei-yu and late season reveals that the percentage of incipient lows developing to TC intensity associated with the mei-yu front is 64.7 % (11/17), which is much higher than the 25 % (11/44) of these associated with the Borneo vortex during the late season. In addition, the average formation time (from 25kt to TS) of a typical front-type case is 47 h, which is indicative of a weak and slow-developing formation. However, of the formation time of semi-stationary cases during the late season is only 28.3 h, which is a weak but faster-developing formation. In general, the average formation time of WNP cases during the winter period is 36.4 h, which is also slower-developing than those of the semi-stationary case associated the Borneo vortex.

Liebmann et al. (1994) showed that the ratios of storms and typhoons formed per TD are the same in the convective phase as they are in the dry phase of the MJO, but they did not include nonformation cases because the identification of incipient disturbance is highly subjective. The probability of incipient vortex formations when the MJO is present is more than twice as when the MJO is absence (Fig. 10b). Importantly, formation is from a stochastic process to physical deterministic process when intensification, which are different scenarios and mechanisms. The stronger equatorial westerly during the active MJO period would produce stronger cyclonic shear vorticity thus is favorable for triggering more convection activity and more vortex formations (Fig. 3c). However, more vortices or cloud clusters is not necessarily more favorable for an incipient vortex to organize into a TC. Therefore, the probability for an incipient vortex to become a TC is actually higher during the non-MJO period in the SCS during the late season. Such feature suggests that the TC formation in the SCS during the late season is like a stochastic process. Nonetheless the environment for formations reveals that the low level relative vorticity and humidity during initial formation period are already significantly different from that for nonformations. Thus the favorable setup of synoptic environment is still a precursor to determine the cloud cluster further development.

6. ACKNOWLEDGEMENT

We gratefully acknowledge the support of our sponsors, National Science Council and Civil Aeronautics Administrator, Taiwan.

REFERENCES

Chang, C. P., J. E. Erickson and K. M. Lau, 1979: Northeasterly cold surges and near-equatorical disturbances over the winter MONEX area during December 1974. Part I: Synoptic aspects. *Mon. Wea. Rev.*, **107**, 812-829.

------, C.-H. Liu, and H.-C. Kuo, 2003 : Typhoon Vamei: An equatorial tropical cyclone formation. *Geophys. Res. Lett.*, **30**, 1151-1154.

------, P. A. Harr, and H.-J. Chen, 2005: Synoptic disturbances over the equatorial South China Sea and western maritime continent during boreal winter. *Mon. Wea. Rev.*, **133**, 489–503.

Liebmann, B., H. H. Hendon, and J. D, Glick, 1994: The relationship between tropical cyclones of the Western Pacific and Indian Oceans and the Madden-Julian oscillation. *J. Meteor. Soc. Japan*, **72,** 401-412.

Lee, C.-S., Y.-L. Lin , and K. K. W. Cheung, 2006: Tropical cyclone formations in the South China Sea associated with the mei-yu front. *Mon. Wea. Rev.*, **134**, 2670-2687.

------, K K. W. Cheung, J. S. N. Hui, R. L. Elsberry, 2008: Mesoscale features associated with tropical cyclone formations in the western North Pacific. *Mon. Wea. Rev.*, **136**, 2006-2022.

Maloney, E. D., and D. L. Hartmann, 2000: Modulation of eastern North Pacific hurricanes by the Madden–Julian oscillation. *J. Climate*, **13**, 1451–1460.

McBride, J. L. and R. Zehr, 1981: Observational analysis of tropical cyclone formation. Part II: Comparison of non-developing verse developing systems. *J. Atmos. Sci.*, **38**, 1132–1151.

Wheeler, M. C., and H. H. Hendon, 2004: An all-season real-time multivariate MJO index: Development of an index for monitoring and prediction. *Mon. Wea. Rev.*, **132**, 1917-1932.

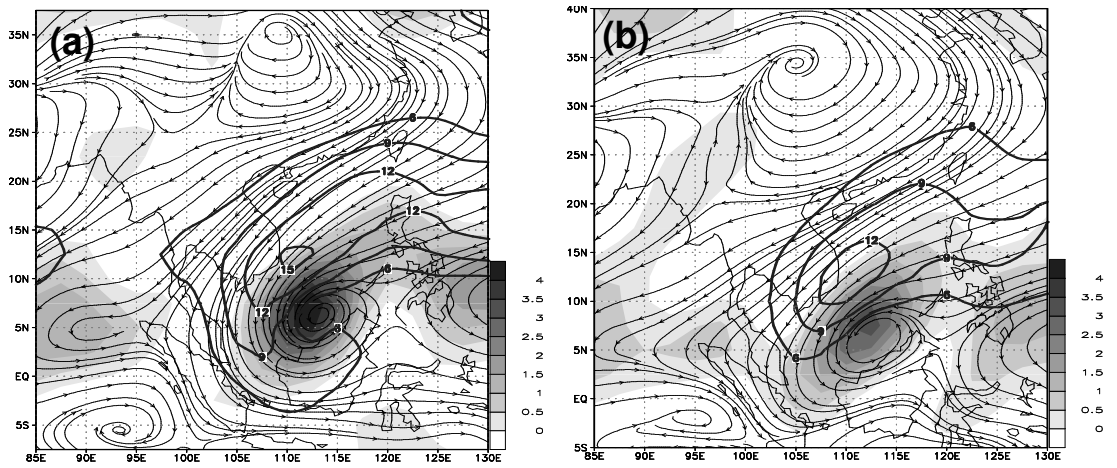

FIG. 1. The 925-hPa flow field for (a) formations and (b) nonformations at 925 hPa. At 48 h. The heavy contours are isotachs (minimum wind speed is 6 m s^{-1} with interval of 3 m s^{-1}). Shadings show positive relative vorticity (interval: 0.5×10^{-5} s^{-1}).

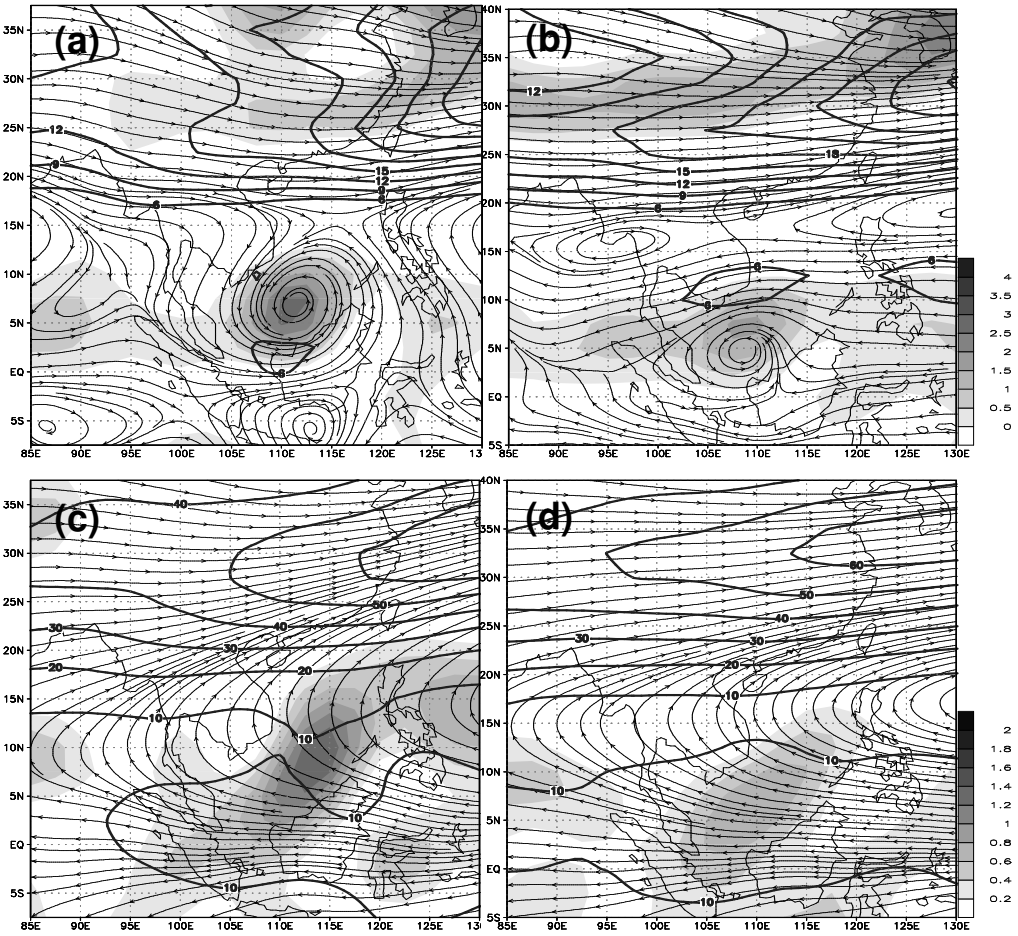

FIG. 2. The 48 h composite in formations (left) and nonformations (right) at (a), (b) 500; and (c), (d) 200 hPa. The heavy contours are isotachs showing wind speeds greater than 6 (10) m s^{-1} with interval of 3 (10) m s^{-1} at 500 (200) hPa. Shadings show positive relative vorticity at 500 hPa or positive divergence at 200 hPa (interval: 0.5×10^{-5} s^{-1} for upper and 0.2×10^{-5} s^{-1} for lower).

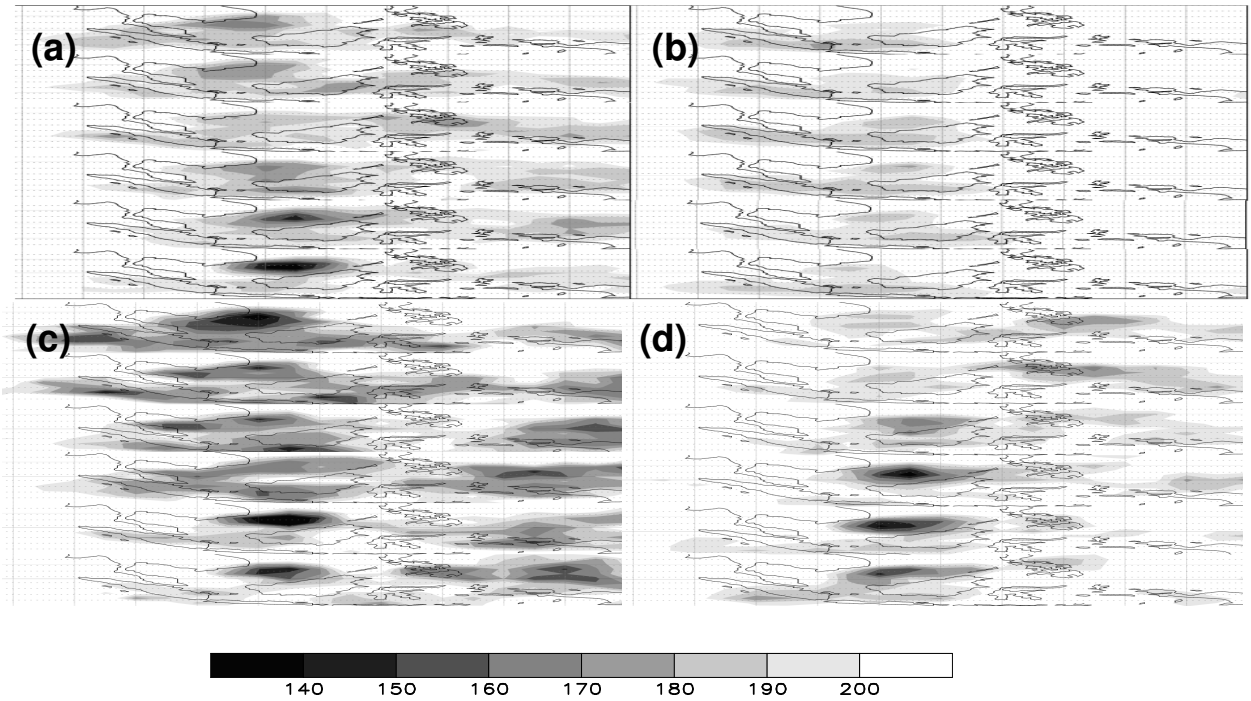

FIG. 3. Composite OLR (W m^{-2}) distribution from three days before to two days after of the zero-reference time for the (a) formations and (b) nonformations. During (c) MJO, (d) non-MJO period for the formations.

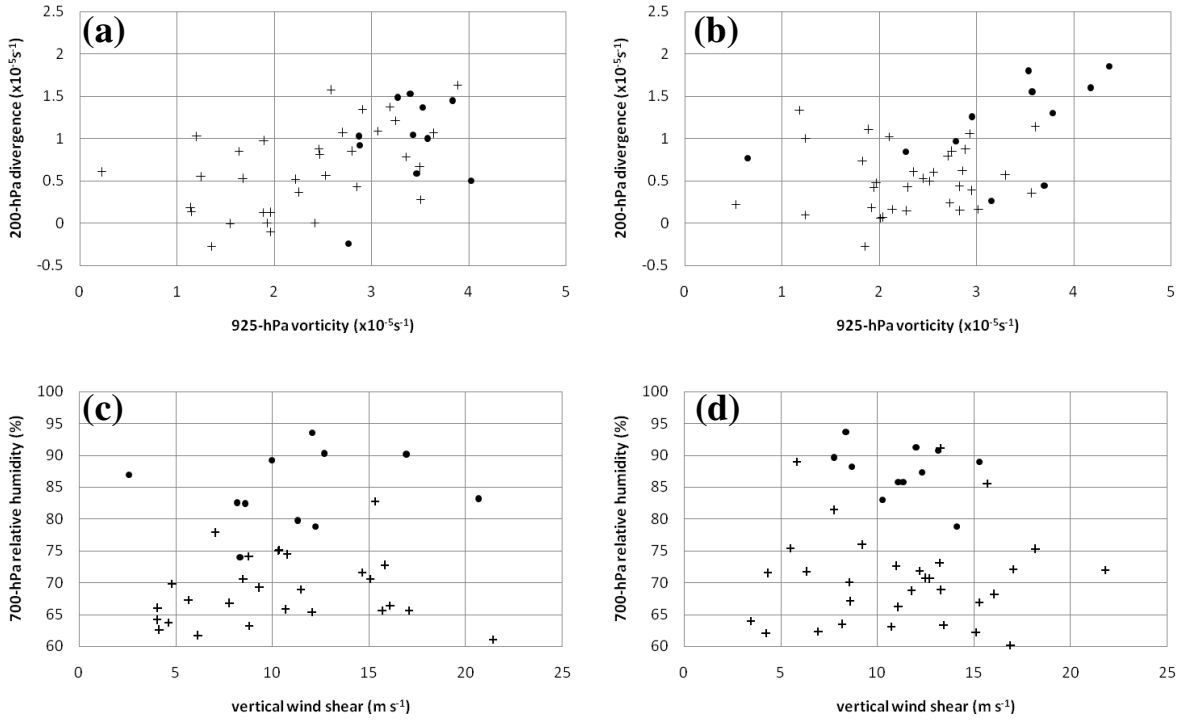

FIG. 4. Scatter plots of formation (dot) and nonformation (cross). (a), (b) 925-hPa vorticity verse 200-hPa divergence; (c), (d) vertical wind shear verse 700-hPa relative humidity. (a), (c) at 24h ; (b), (d) at 72h.

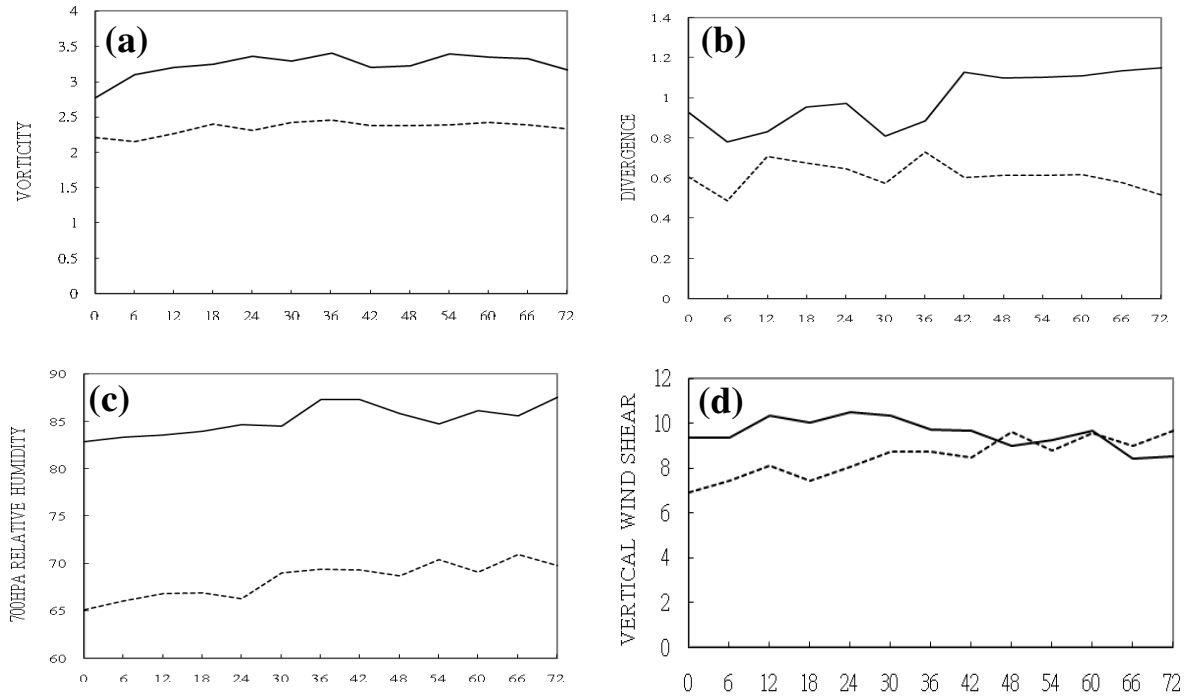

FIG. 5. (a) Averaged 925-hPa relative vorticity (unit: 10^{-5} s^{-1}), (b) 200-hPa divergence (unit: 10^{-5} s^{-1}), (c) 700-hPa relative humidity (unit: %) (d) 200–850-hPa vertical wind shear magnitude (unit: m s^{-1}) for the formation (solid) and non-formation (dashed) cases.

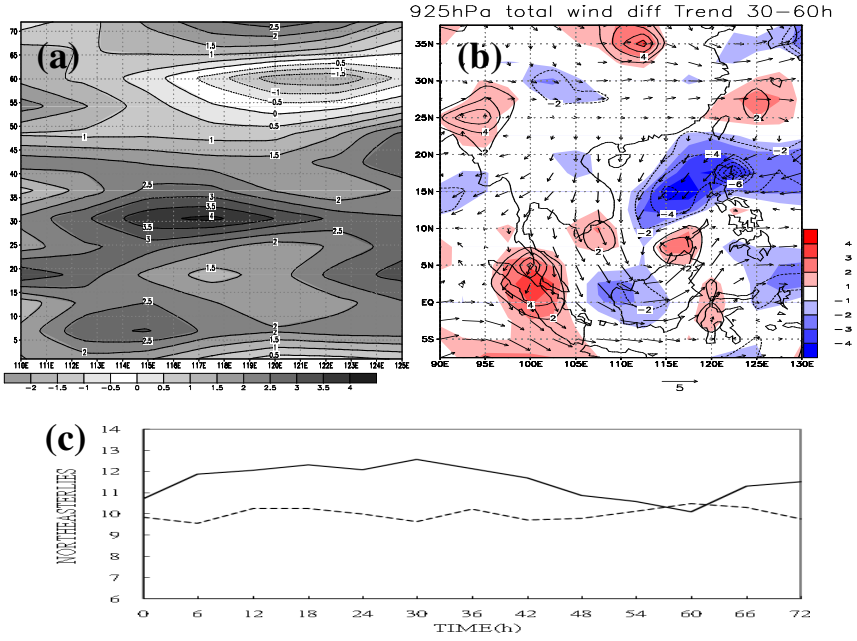

FIG. 6. (a) The 925-hPa northeasterly difference (formation minus nonformation) at 7.5° north of disturbance center, (b) tendency of wind speed (shaded; unit: m s^{-1}) from 30 h to 60 h ,wind vector is the mean flow, inside the contour is passing the 95% confident level and (c) the time series assessing the quantity of the aerial average of the northeasterly (m s^{-1}) for 5°×15° area that is 5° north of disturbance center for formation and nonformation cases.

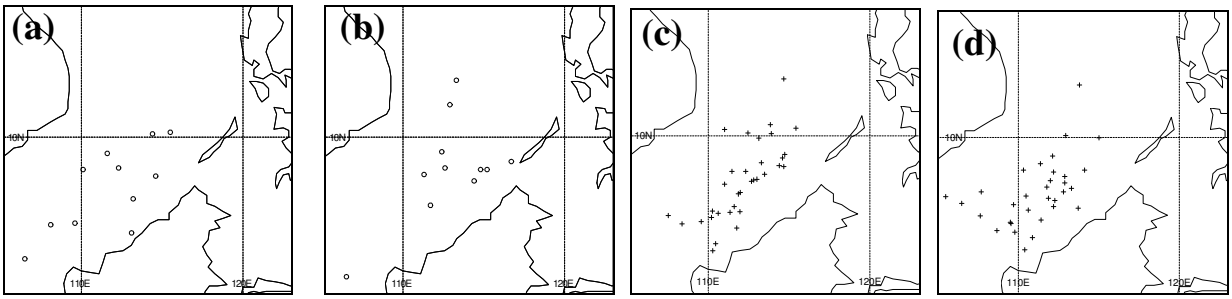

FIG. 7. The position for formations at (a) 30, (b) 60 h and for nonfomations at (c) 30, (d) 60 h after surface closed-isobar feature is identified.

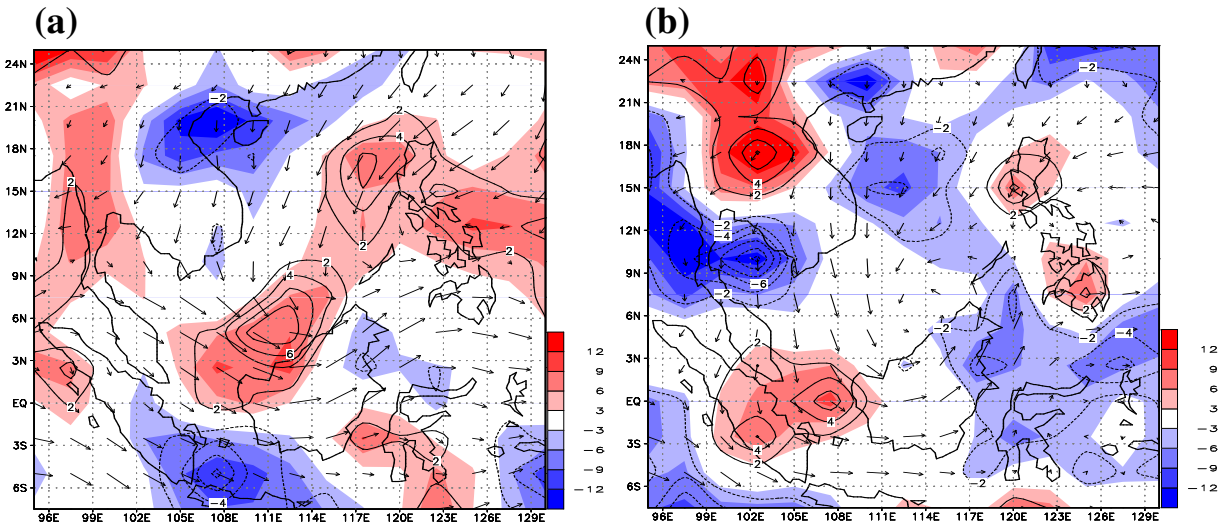

FIG. 8. The tendency difference (formation minus nonformation) of 925-hPa relative humidity (shading; unit:%) from (a) 0 to 30 h and (b) 30 to 72 h. Wind vector is the mean flow and inside the contour is passing the 95% confident level.

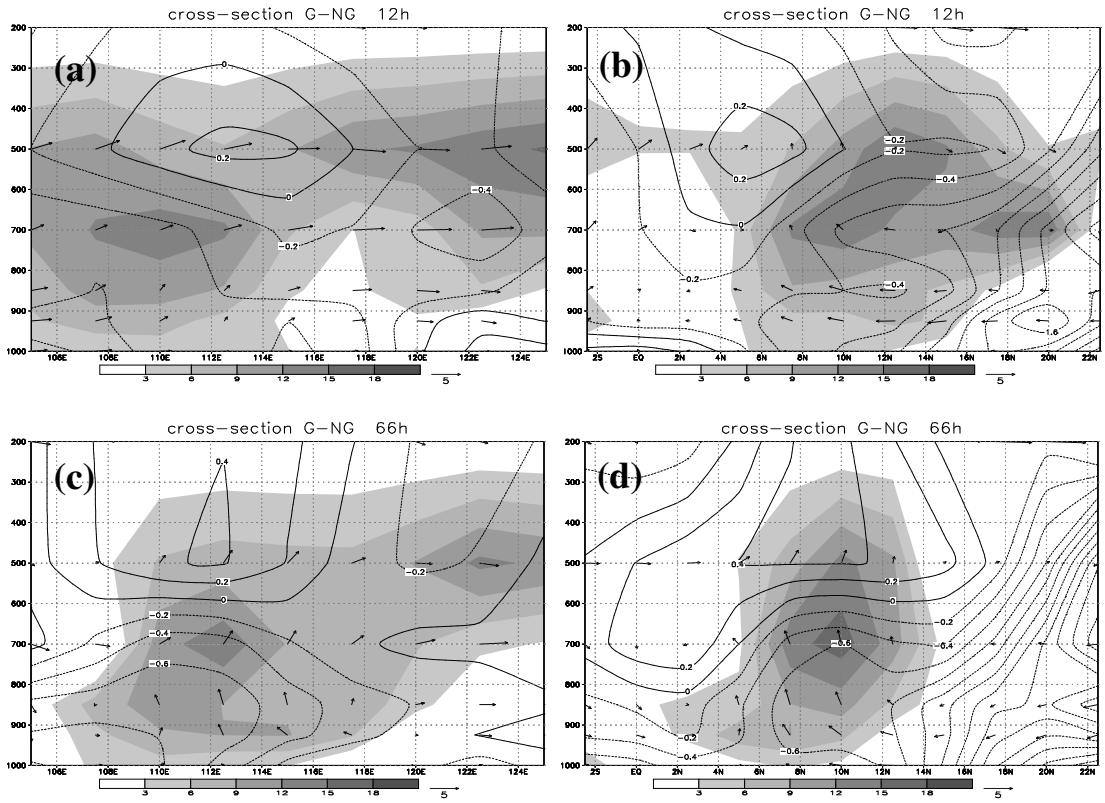

Fig. 9 The difference (formation minus nonformation) of temperature (contour) and humidity (shaded) of vertical cross section along (a), (c) 7.5°N and (b), (d) 112.5°E. (a) and (b) are at 12 h, (c) and (d) are at 66 h.

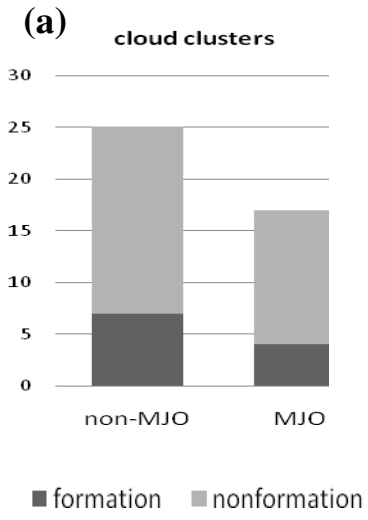

(b)

	non- MJO	MJO
no- vortex	2373	361
vortex	109	40
% of total days	4.4%	10%

FIG. 10. The TC formation probability with the MJO and non-MJO in terms of (a) cloud clusters and (b) incipient vortex formation probability.